Journal of Materials Science: Materials in Electronics (2019) 30:19404–19414
https://doi.org/10.1007/s10854-019-02302-z

Multifunctional performance derived by Eu doping in $(Ba_{0.85}Ca_{0.15})(Ti_{0.9}Hf_{0.1})O_3$ lead-free ceramics

Shanshan Zhang[1] · Bijun Fang[1] · Xiangyong Zhao[2] · Shuai Zhang[1] · Zhihui Chen[1] · Jianning Ding[1,3]

Received: 19 June 2019 / Accepted: 30 September 2019 / Published online: 8 October 2019

Abstract
Multifunctional perovskite oxides $[(Ba_{0.85}Ca_{0.15})_{1-x}Eu_x](Ti_{0.9}Hf_{0.1})O_3$ (Eu-BCTH) were prepared by the solid-state reaction method, and the effects of Eu doping on structure, density, and performance were studied. The Eu-BCTH ceramics sintered at 1450 °C for 3 h exhibit a near-pure perovskite structure accompanied by high relative density and densified microstructure morphology. The Eu-doped BCTH ceramics present complicated dielectric behaviour, that is, normal ferroelectrics accompanied by slight diffusive ferroelectric phase transition characteristics. Excellent ferroelectricity and piezoelectricity can be obtained in the Eu-doped BCTH ceramics simultaneously, which present significant dependency on the Eu doping content. Under 457-nm light excitation, the Eu-BCTH ceramics emit strong red fluorescence centering around 689 nm, relating to the $^5D_0 \rightarrow {}^7F_4$ electron transition, accompanied by several weak fluorescence emissions. The 0.5 mol% Eu-doped BCTH ceramics present excellent piezoelectric and florescent properties simultaneously.

1 Introduction

Multifunctional materials and components have gathered focused attention in science and engineering fields to meet the requirements of miniaturization and intellectualization of high-tech electronic devices, and increase system-level multifunctionality and efficiency [1, 2]. Normally, multifunctionality is stimulated by multiple driving force, including temperature, stress, electromagnetic wave, field, et al., and their combination, in novel materials and structures. Besides generating novel multiple performances and functions, which may be absent in original unifunctional materials, weight, volume, connectors, production cost, etc., can be saved, which provide enhanced tailorable to applications and are very important in New Technology Age.

Among versatile multifunctional materials, rare-earth elements tailored ferroelectrics have attracted our attention since donor-doping improved piezoelectricity and remnant polarization enhanced fluorescence performance can be induced by the lanthanide element doping (i.e., typical multifunctionality) [3, 4]. The improved fluorescent and piezoelectric properties can be attributed to the ample inner-layer 4f and 5d electron states and donor doping characteristics of the rare-earth elements [1, 5, 6].

For fluorescent and piezoelectric multifunctional materials, their performances are influenced fundamentally by rare-earth elements species and concentrations, ferroelectric host materials, ceramic processing, and so on.

Compared with other rare-earth cations, Eu^{3+} has abundant electron levels, whose excitation spectra and luminescent spectra relating to the ground state level are non-degenerate owing to the even number of 4f electrons ($4f^6$ configuration) [7]. Furthermore, the crystal-field perturbation induced by the host matrix can lift degeneracy of the $^{2S+1}L_J$ levels [7], leading to promising versatile applications

✉ Bijun Fang
fangbj@cczu.edu.cn

✉ Xiangyong Zhao
xyzhao@shnu.edu.cn

✉ Jianning Ding
dingjn@cczu.edu.cn

1 School of Materials Science and Engineering, Jiangsu Collaborative Innovation Center of Photovoltaic Science and Engineering, Jiangsu Province Cultivation Base for State Key Laboratory of Photovoltaic Science and Technology, National Experimental Demonstration Center for Materials Science and Engineering, Changzhou University, Changzhou 213164, China

2 Key Laboratory of Optoelectronic Material and Device, Department of Physics, Mathematics & Science College, Shanghai Normal University, Shanghai 200234, China

3 School of Material Science and Engineering, Jiangsu University, Zhenjiang 212013, China

in the fields of display, solid-state lighting, optoelectronics, etc. [8].

Owing to environmental concerns and legislative restrictions, lead-free ferroelectrics have become topics of research interest as host materials since the remnant polarization [3, 4] and random electric-field [9] can enhance the fluorescent performance of rare-earth luminescent materials by influencing the crystal field. The compound $(Ba_{1-y}Ca_y)(Ti_{1-x}Hf_x)O_3$ (BCTH) has potential for practical applications since it was reported by Zhou et al. [10], which exhibits excellent piezoelectricity and ferroelectricity depending on composition, and arouses research booming subsequently [11–13]. Piezoelectricity improvement caused by donor doping and photoluminescence performance enhancement induced by ferroelectricity coupling is anticipated in rare-earth doped BCTH owing to the remnant polarization, internal electric-field, and the change in local crystal symmetry and crystal-field [1, 3, 4, 9].

In this work, Eu-doped $[(Ba_{0.85}Ca_{0.15})_{1-x}Eu_x](Ti_{0.9}Hf_{0.1})O_3$ (Eu-BCTH) lead-free multifunctional ceramics were prepared by conventional ceramic processing since the solid-state sintering method is simple and low-cost, and the Eu concentration and sintering conditions can be tailored easily [10–13]. The effects of Eu doping content on crystal structure and morphology, elemental distribution, and multifunctional performances were investigated, and the underlying mechanisms of ferroelectricity coupling and photoluminescence performance enhancement were identified.

2 Experimental procedures

Eu-doped $(Ba_{0.85}Ca_{0.15})(Ti_{0.9}Hf_{0.1})O_3$ (BCTH) lead-free multifunctional ceramics were prepared by the solid-phase method according to the formula $[(Ba_{0.85}Ca_{0.15})_{1-x}Eu_x](Ti_{0.9}Hf_{0.1})O_3$ (Eu-BCTH) without considering charge compensation using carbonates and oxides as raw materials. Stoichiometric well mixed reagents of $BaCO_3$, $CaCO_3$, Eu_2O_3, TiO_2, and HfO_2 with full drying were calcined at 1350 °C for 3 h with repeated grinding and calcining to ensure full decomposition of carbonates and solid-state reaction. The Eu-doped BCTH ceramics were sintered at 1450 °C for 3 h with a separate decarbonation process after granulation and cold-pressing covered with calcined powder of the same composition.

Rigaku D/max-2500/PC X-ray diffractometer and Rigaku SmartLab X-ray diffractometer (XRD), and JEOL JSM-IT100 InTouchScope™ scanning electron microscope (SEM) were used to characterize the crystal phase structure, and grains morphology and elementals surface distributions of the synthesized Eu-BCTH ceramics, respectively. Luminescent images, photoluminescence properties, and luminescent lifetime were analysed using a Nikon Inverted Research Microscope Eclipse Ti-S, PerkinElmer LS 45 fluorescence spectrometer and Edinburgh FS5 fluorescence spectrometer, respectively, using polished ceramics [14, 15]. Dielectric, piezoelectric and ferroelectric measurement systems were used to characterize electrical properties using silver-electroded ceramics after manual coating and silver-firing at 650 °C for 30 min [16].

3 Results and discussion

Figure 1 shows XRD patterns of the Eu-BCTH ceramics. Minor impurities exist in most of the sintered Eu-doped BCTH ceramics, except for the 0.5 mol% Eu-doped BCTH ceramic; therefore, the phase structure of the Eu-BCTH ceramics deserves further optimization. Such impurities will influence the physical performance change characteristics, but not significantly since the electrical and optical properties of the Eu-BCTH ceramics can be comparable to many similar ceramics reported. On the whole, a near-pure perovskite structure is obtained, and the ceramics seemly present rhombohedral or pseudo-cubic systems in the full XRD patterns since the {110}, {210} diffraction reflections exhibit rather sharp and symmetric singlet peaks. Almost no impurities are detectable with varying the Eu doping content. This composition was chosen as the matrix as it is located around the distinguished morphotropic phase boundary (MPB), which tends to present excellent physical performance [10–13]. The existence around the MPB region can be confirmed in magnified XRD patterns. Doublet splitting of the {200} diffraction reflection and triplet splitting of the {310} diffraction reflection become more evident as the Eu doping content increases in the Eu-doped BCTH ceramics. The splitting in the 0.1 mol% Eu-doped BCTH ceramics is more clearly, which can be deconvoluted and indexed as the tetragonal $(002)_T$ and $(200)_T$, the tetragonal $(301)_T$ and $(310)_T$, and the rhombohedral $(310)_R$; that is, the coexistence of tetragonal and rhombohedral phases (or orthorhombic phase), correlating with the XRD equipment used (Rigaku SmartLab X-ray Diffractometer) and the crystal distortion caused by Eu doping. Further structural refinement will provide more precise structural information; for example, in a correlative composition system of $(Ba_{0.7}Ca_{0.3}TiO_3)$–$(BaZr_{0.2}Ti_{0.8}O_3)$ (BCZT), an intermediate orthorhombic ferroelectric phase with lower symmetry is detected by high-resolution synchrotron X-ray diffraction combined with Rietveld refinement, first-principles density-functional calculations, Landau-Devonshire theory, and Raman spectroscopy [17–19]. The intermediate orthorhombic phase converges polymorphic phase coexistence region, degenerates and flattens the critical free energy landscape, and multiplies polarization orientations, leading to enhanced physical properties [17–19].

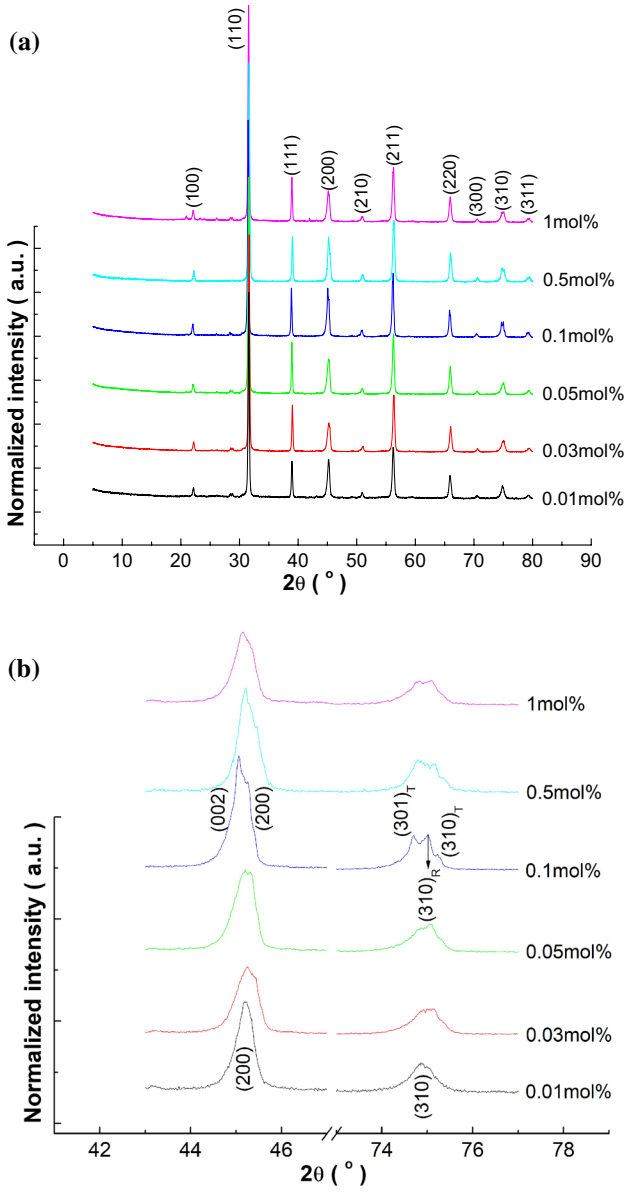

Fig. 1 **a** XRD patterns of the Eu-BCTH ceramics; **b** enlarged XRD patterns around the {200} and {310} diffraction reflections of the Eu-BCTH ceramics

Therefore, the structure of the Eu-BCTH ceramics is refined as pseudo-cubic symmetry with rhombohedral distortion as shown in Table 1. Normally, the cell parameters a and V present a decreasing trend with increasing the Eu doping content until 0.1 mol%, after which there is an almost linear increase until the end concentration of the experiment, which correlates with the differences in valences and ionic radii of the different cations; that is, 1.61 Å, 1.34 Å and 1.12 Å for Ba^{2+}, Ca^{2+}, and Eu^{3+} in 12-fold coordination (Eu^{3+} in 9-fold coordination since it has no data in 12-fold coordination), and 0.51 Å, 0.71 Å and 0.947 Å for Ti^{4+}, Hf^{4+}, and Eu^{3+} in sixfold coordination [20]. Cell distortion is induced by changes in oxygen vacancy concentration due to the generation of complex point charge defects, and the different occupation sites in the perovskite structure. That means that although Eu is designed for A-site doping in the perovskite structure, the real occupation location varies depending on the Eu content and the chemical environmental. Minor interstitial occupation of the perovskite structure is also inevitable. A similar phenomenon is reported by Luo et al., who designed a systematic experimental to investigate the effects of Er occupying sites in $Na_{0.5}Bi_{0.5}TiO_3$ perovskite on the physical properties [21]. In realty, the precise occupying sites of Er doping in the perovskite structure are difficult to control and detect [21].

Although the maximum Eu doping content is set as 1 mol% owing to considering multifunctional physical properties, the sintering capability is improved obviously as shown in Table 1 (all relative densities > 93%). The variation trend of the relative density is similar to that of the cell parameters, partially corroborating the change of Eu occupying sites in the perovskite structure. Therefore, complex point charge defects are produced, as shown by the Kröger-Vink notation system; that is, $Eu_2O_3 \xrightarrow{BCTH} 2Eu^{\bullet}_{Ba/Ca} + V''_{Ba/Ca} + 3O^{\times}_{O}$ and $2Eu_2O_3 \xrightarrow{BCTH} 4Eu'_{Ti/Hf} + 2V^{\bullet\bullet}_{O} + 4O^{\times}_{O} + O_2\uparrow$ [22, 23]. Furthermore, the charge balance was not considered when designing the composition formula in this work, and this induced perovskite cell distortion and significantly

Table 1 Cell parameters and density of the Eu-BCTH ceramics

Eu content (mol %)	a = b = c (Å)	α = β = γ (°)	Cell volume (Å^3)	Relative density (%)
0.01	4.00126 ± 0.001209	89.8597 ± 0.044818	64.06	95.7
0.03	4.00216 ± 0.00126	89.8548 ± 0.046507	64.1	94.8
0.05	4.00121 ± 0.000776	89.9235 ± 0.031341	64.06	94.1
0.1	3.99584 ± 0.000579	89.9355 ± 0.023528	63.8	94.4
0.5	4.00432 ± 0.001476	89.8159 ± 0.05449	64.21	93.2
1	4.00722 ± 0.000405	90.0348 ± 0.009563	64.35	94.4

influenced the physical performance of the synthesized Eu-BCTH ceramics.

The high densification is confirmed by SEM observations. Before SEM measurements, the Eu-BCTH ceramics were thermal etched at 1350 °C for 30 min. Figs 2, 3 show SEM images and elemental maps of the 0.5 mol% Eu-doped BCTH ceramics as an example. Normal distribution of grains is observed with a grain size concentrated around 5.8–13 μm, correlating with the inhibition of grain growth induced by the Eu doping as compared with the BCTH ceramics without rare-earth doping [10–13]. The grains present nearly rounded corners, although the grains shape is irregular, indicating the partial role of a liquid-phase sintering mechanism. The compact grains morphology supports their high relative density. The clear grain boundaries, enlarged porosity around grains junctions, and some misty matter covering above the ceramics' surface relate to the thermal etching process and the free surface without grinding and polishing used for the SEM measurement.

For elementals surface analysis, the grain junctions of three grains and a large grain were measured to detect the distributions inside grains and around grain boundaries. Owing to the low doping content of Eu and its excited electron energy level that is overlapped by other elements, the Eu surface distribution cannot be detected by energy dispersive spectroscopy (EDS). Fortunately, this deficiency can be compensated for by using luminescent images detected by fluorescence microscopy as discussed below. Overall, the elemental distributions both inside grains and around grain boundaries are generally homogenous, especially in the image of combined distributions of Ba, Ca, and Ti in the large grain (Fig. 3). The strong contrast around grain boundaries (i.e., the light color indicating lower element concentrations) correlates with the thermal etching process since the elements located around grain boundaries evaporate most easily owing to their disordered arrangement, greater number of defects, and high energy.

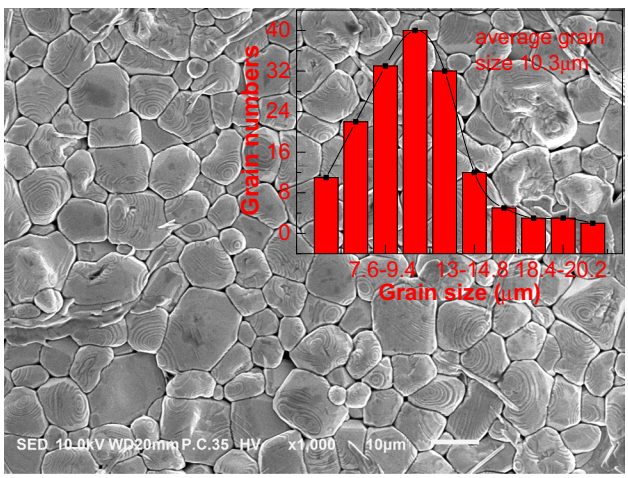

Fig. 2 SEM image of the 0.5 mol% Eu-doped BCTH ceramics. Inset shows histogram of grains size distribution

For electronic applications, high resistance is a basic performance requirement. As shown in Table 2, all of the Eu-BCTH ceramics present high insulation, normally larger than 10^{10} Ω·cm. The largest resistivity reaches 6.850×10^{11} Ω·cm for the 0.01 mol% Eu-doped BCTH ceramics, and high piezoelectricity can be expected. The resistivity does not show simple change regularity, which can be attributed to the complex change of bulk density, microstructural morphology, cell parameters, etc., complicated point defects formation mechanisms, and different substitutional and minor interstitial solution (i.e., occupying A-site or B-site, and minor interstitial site of the perovskite structure) in the Eu-doped BCTH ceramics induced by Eu doping.

Figure 4 shows dielectric-temperature spectra of the Eu-BCTH ceramics measured at 10 kHz. Although the Eu doping content is limited, the dielectric response characteristics [i.e., the dielectric peaks width, the value of the dielectric constant maximum (ε_m), the temperature corresponding to the ε_m value (T_C), and the dielectric frequency dispersion character] change greatly with increasing the Eu concentration. Although the low-temperature rhombohedral-orthorhombic-tetragonal (R-O-T) phase transitions is not observed in the dielectric permittivity curves due to the equipment limitation, the apparent decrease of the dielectric loss tangent around room temperature in the dielectric loss-temperature curves as shown in Fig. 4 can be attributed to the O–T phase transition [12]. Combined with the data in Table 3, the 0.5 mol% Eu-doped BCTH ceramics exhibit excellent dielectric properties with relatively large ε_m value and high T_C temperature simultaneously.

The frequency influence and dielectric behaviour fitting were considered using the 0.5 mol% Eu-doped BCTH ceramics as an example (Figs. 5, 6, 7). No apparent dielectric frequency dispersion is observed, in which the ε_m value decreases from 11668.6 to 10862.1 between 100 Hz and 2 MHz, whereas the T_C temperature remains at 86 °C; the full-width at the half dielectric peak maxima at 10 kHz is 26 °C. The temperatures of the dielectric loss maxima are lower than their corresponding T_C temperatures, and the dielectric loss frequency dispersion is clear (Fig. 5). The abnormally rapid increase in dielectric loss above the T_C temperature at low frequencies confirms the formation of complex point charge defects of $Eu^{\bullet}_{Ba/Ca}$, $V''_{Ba/Ca}$, $Eu'_{Ti/Hf}$, and $V^{\bullet\bullet}_{O}$, which present hopping-jumping type conduction behaviour and can be attributed to a thermally activated conduction mechanism [24].

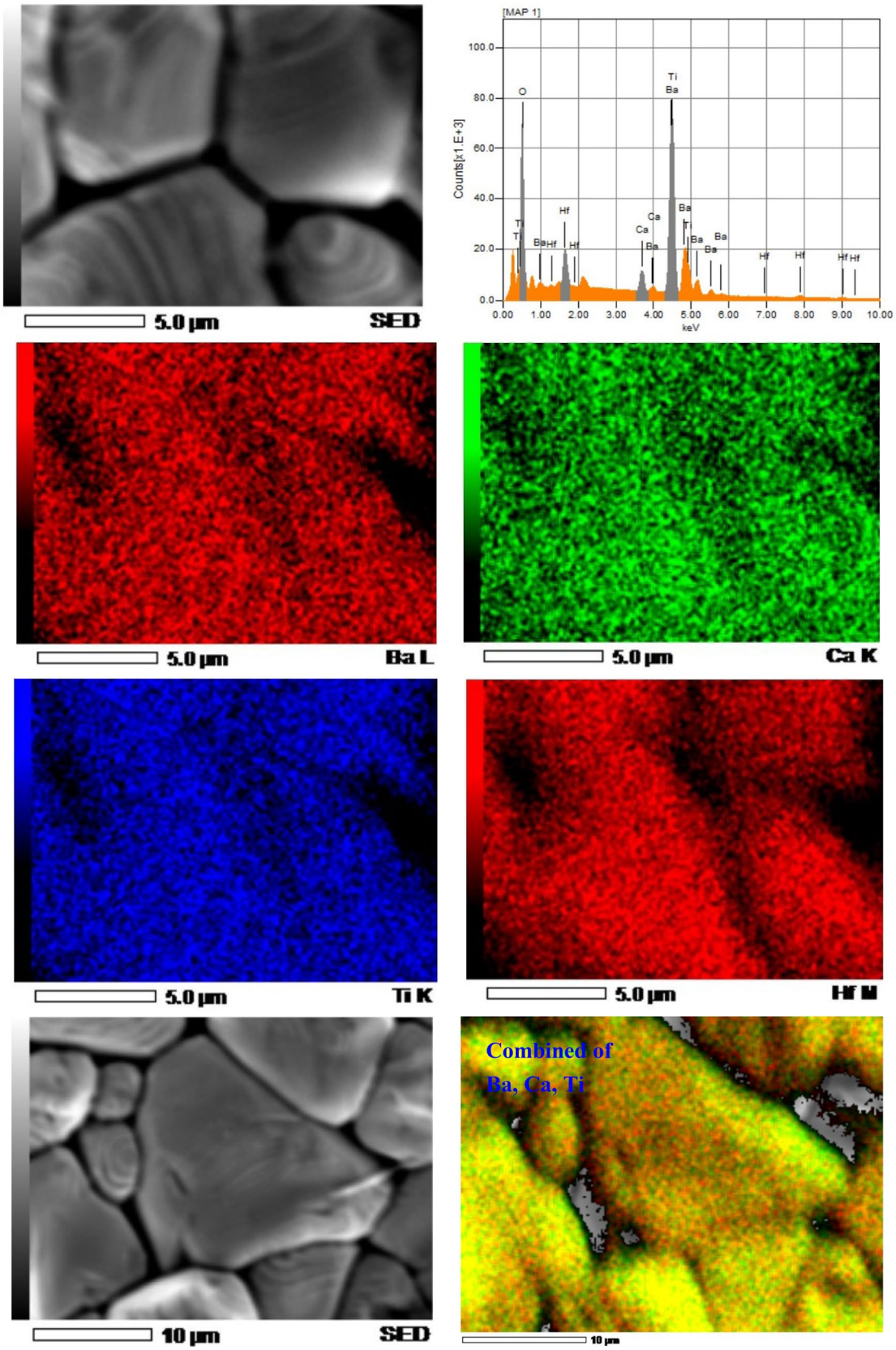

Fig. 3 SEM morphology region for Energy Dispersive X-ray analysis (EDX), EDX energy spectrum and images of elementals surface analysis locating around grain boundary and within grains of the 0.5 mol% Eu-doped BCTH ceramics

Table 2 Resistivity of the Eu-BCTH ceramics

Eu content (mol %)	0.01	0.03	0.05	0.1	0.5	1
Resistivity (Ω·cm)	6.850E+11	3.287E+10	3.052E+11	6.972E+10	9.935E+10	1.202E+11

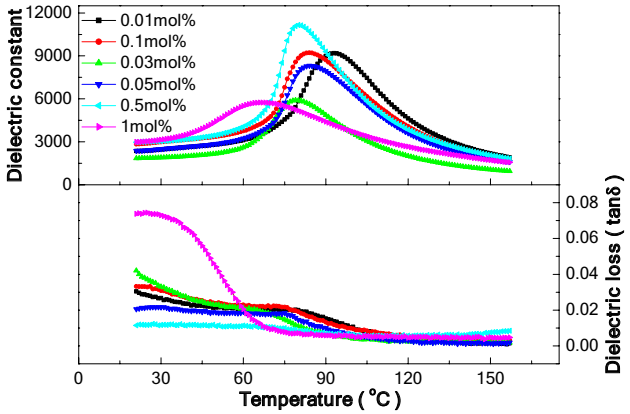

Fig. 4 Temperature dependence of dielectric constant and loss tangent of the Eu-BCTH ceramics measured at 10 kHz upon heating

Table 3 ε_m and T_C of the Eu-BCTH ceramics at 10 kHz

Eu content (mol %)	ε_m	T_C (°C)
0.01	9186.6	93
0.03	5902.8	87
0.05	8313.3	90
0.1	9219.4	88
0.5	11149.8	86
1	5744.1	70

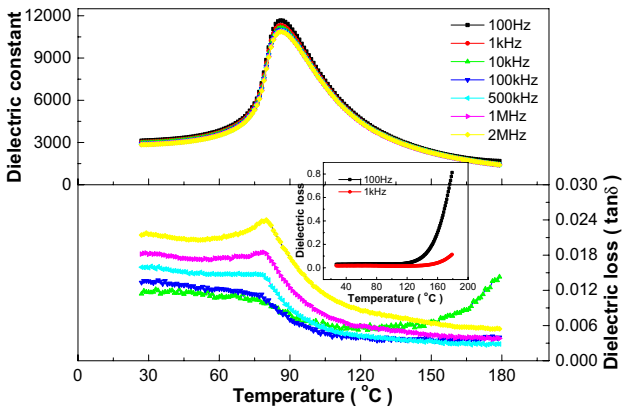

Fig. 5 Temperature dependence of dielectric constant and loss tangent of the 0.5 mol % Eu-doped BCTH ceramics measured at several frequencies upon heating

Curie–Weiss law fitting $\varepsilon = C/(T - T_0)$ and exponential law fitting $1/\varepsilon - 1/\varepsilon_{max} = (T - T_m)^{\gamma}/C'$ provide further method to analyse the

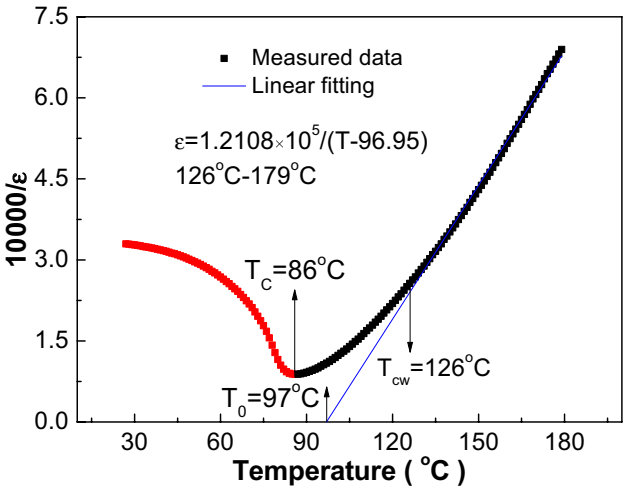

Fig. 6 Curie-Weiss fitting of dielectric behavior above T_C of the 0.5 mol % Eu-doped BCTH ceramics using 1 kHz data

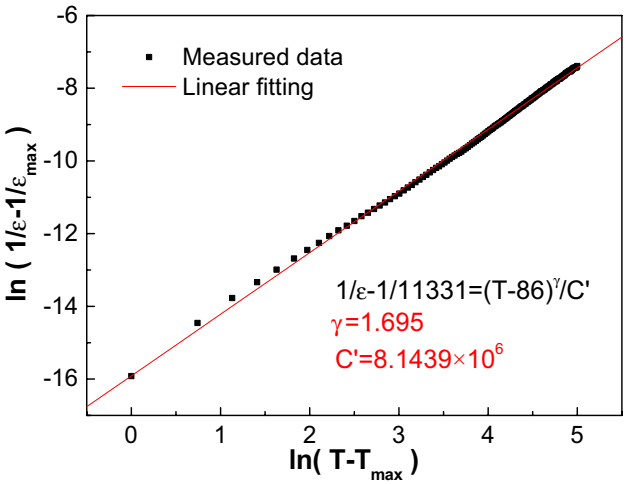

Fig. 7 Quadratic law fitting of dielectric behavior above T_C of the 0.5 mol % Eu-doped BCTH ceramics using 1 kHz data

ferroelectric behaviour characteristics [25]. Both laws can fit the dielectric response behaviour of the 0.5 mol% Eu-doped BCTH ceramics, in which the fitting equations are $\varepsilon = 1.2108 \times 10^5/(T - 96.95)$ and $1/\varepsilon - 1/11331 = (T - 86)^{1.695}/8.1439 \times 10^6$, respectively; however, they are not in complete agreement. For the former, the Curie constant has a magnitude of 10^5, indicating normal ferroelectric behaviour, whereas the Curie–Weiss law is obeyed within 126–179 °C and the T_{cw} temperature (i.e.,

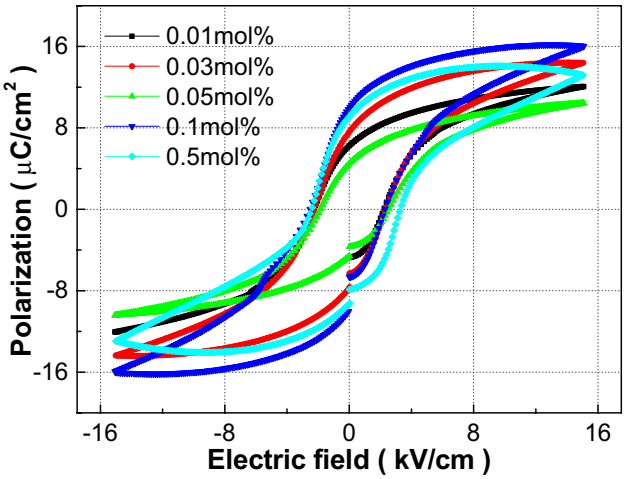

Fig. 8 P-E hysteresis loops of the Eu-BCTH ceramics measured at 15 kV/cm and 10 Hz

the beginning temperature that the Curie–Weiss law is obeyed) is significantly higher than the T_C temperature, presenting a deviation from the Curie–Weiss law. For the latter, the fitted diffuseness coefficient is only 1.695, suggesting non-typical relaxor ferroelectric characteristics. Therefore, the Eu-doped BCTH ceramics present complicated dielectric behaviour, i.e., normal ferroelectrics accompanied by slight diffusive ferroelectric phase transition characteristics.

Figure 8 shows polarization–electric field (P–E) hysteresis loops of the Eu-doped BCTH ceramics measured at room temperature. Owing to the formation of point defects in the 1 mol% Eu-doped BCTH ceramics, their P–E loop cannot be obtained even with a 15 kV/cm electric field. For the other compositions, the P–E loops are rather symmetric and saturate. With increasing the Eu doping content, the remnant polarization tends to increase and reaches maximum value at 0.1 mol% Eu, then decreases with further increase in the Eu doping content, accompanied by slight deformation of the P–E loop around the end parts. The coercive field presents a similar decreasing trend with an increase in the Eu doping content. Such phenomena relate to the formation of complex point charge defects induced by the Eu doping; that is, $Eu^{\bullet}_{Ba/Ca}$, $V''_{Ba/Ca}$, $Eu'_{Ti/Hf}$, and $V^{\bullet\bullet}_{O}$ point defects, which present donor doping characteristics and enhance ferroelectricity. Leakage phenomenon appears in the 0.5 mol% Eu-doped BCTH ceramics as shown by the gap and slight asymmetry of the P-E loop, correlating with the formation of donor-type point defects. Moreover, domain mobility is increased since the free energy for domain rotation and switching is decreased owing to the distortion and relaxation of crystal lattices induced by vacancies, which promotes piezoelectricity [26].

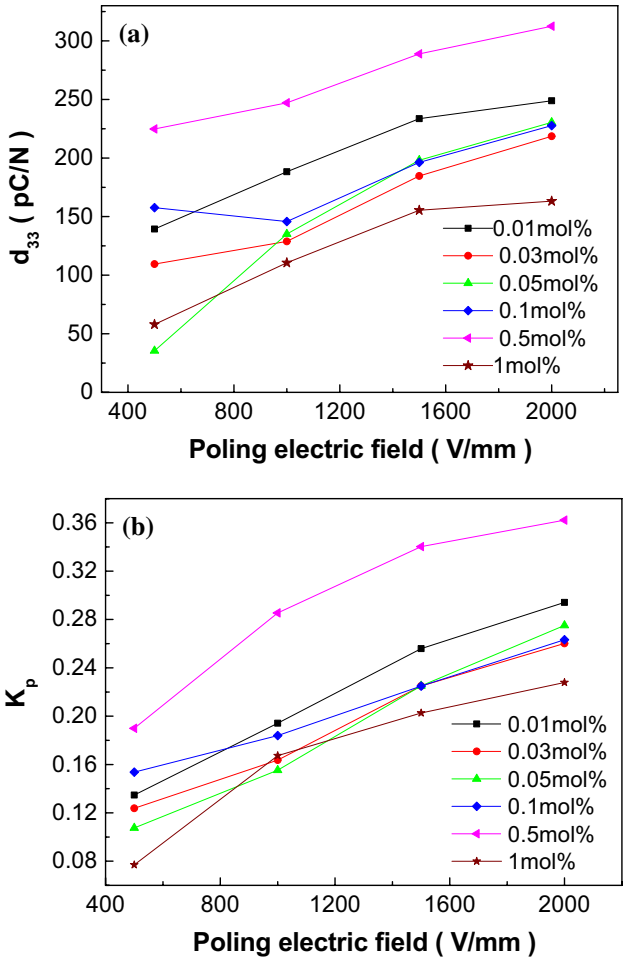

Fig. 9 Poling electric field dependence of **a** piezoelectric constant d_{33} and **b** electromechanical coupling factor K_p of the Eu-BCTH ceramics

The influence of the poling electric field on the piezoelectricity of the Eu-BCTH ceramics is shown in Fig. 9. On the whole, the Eu-BCTH ceramics are susceptible to polarization; at only 500 V/mm, the ceramics obtain relatively high values of the piezoelectric constant d_{33}, which remains almost unchangeable or increases slightly with increasing the electric field depending on the Eu doping content. Such a phenomenon confirms that the enhanced domain mobility is correlated with the point charge defects induced by the Eu doping, and also corresponds to the decreased coercive field E_c (Fig. 8). The largest piezoelectric performance is obtained for the 0.5 mol% Eu-doped BCTH ceramics, with d_{33} and K_p being 317 pC/N and 36.2%, respectively, for poled under 2000 V/mm. The worst piezoelectric performance is observed for the 1 mol% Eu-doped BCTH ceramics, in which the d_{33} value is 163 pC/N and K_p is 22.8%; furthermore, the ceramics cannot be poled by a higher electric field owing to dielectric breakdown. Such phenomena correlate with the change of point charge defects

induced by Eu doping. The Eu cation doping presents donor doping characteristics in the BCTH system, where the piezoelectric constant tends to increase with increasing the Eu doping content via the point defect reaction $Eu_2O_3 \xrightarrow{BCTH} 2Eu^{\bullet}_{Ba/Ca} + V''_{Ba/Ca} + 3O^{\times}_{O}$. However, when the Eu content is too high, oxygen vacancy is generated via the point defect reaction $2Eu_2O_3 \xrightarrow{BCTH} 4Eu'_{Ti/Hf} + 2V^{\bullet\bullet}_{O} + 4O^{\times}_{O} + O_2 \uparrow$, which reunites donor electrons, decreases the piezoelectric constant, and corresponds well with large dielectric loss and inferior ferroelectricity [24].

Unlike the luminescence mechanism of semiconductors, the photoluminescence emission induced by rare-earth doping correlates closely with the specific electron transitions of the 4f or 4f-5d electron layers [5]. Therefore, excitation spectra were measured to determine the effective excitation light wavelength using the 0.5 mol% Eu-doped BCTH ceramics as an example (Fig. 10). Strong excitation light is centred at 457 nm, which correlates with the electron transition of Eu^{3+} from the ground state to the 5d electron level, indicating that 457 nm light can excite the Eu-BCTH ceramics effectively. As compared with the $Na_{0.5}Bi_{0.5-x}Eu_xTiO_3$ (NBT-Eu) powders prepared using the hydrothermal method, a slight blue-shift occurs in the excitation light [27], which can be attributed to the differences in the microstructure morphology caused by the different synthesis methods and internal bias fields induced by different ferroelectric hosts with different crystal fields and local symmetry [1].

The multifunctional photoluminescence emission in the Eu-BCTH ceramics is derived from rare-earth doping, with the emission intensity influenced by the concentration of Eu and the crystal-field symmetry of the ferroelectric hosts [1], as shown in Fig. 11. Strong photoluminescence emission spectra are excited by Eu doping, and the

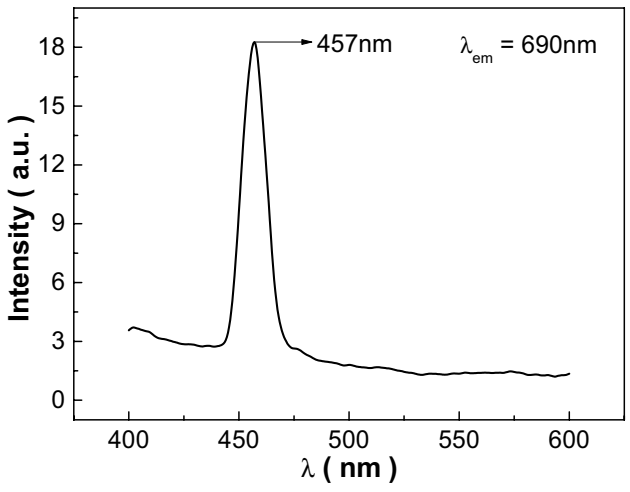

Fig. 10 Photoluminescence excitation spectrum of the 0.5 mol % Eu-doped BCTH ceramics under 690 nm monitoring light

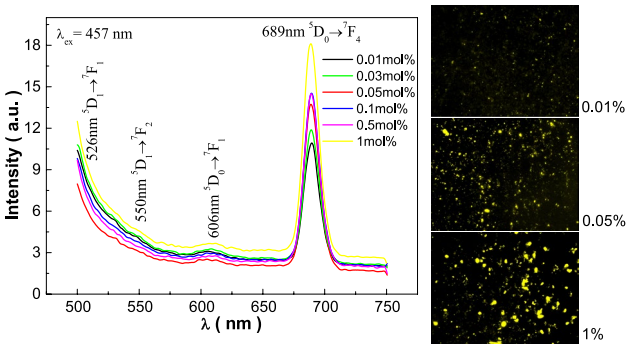

Fig. 11 Photoluminescence emission spectra of the Eu-BCTH ceramics excited under 457 nm light. Insets show luminescent images of three typical compositions

electron transitions are clearly affected owing to the change of atomic displacement and the local lattice environment [1] induced by Eu substitution. Normally, four photoluminescence emission peaks can be excited [5, 7], as reported for the NBT-Eu ceramics prepared via the hydrothermal method [27]; however, in this work, only two emission peaks are apparent for the Eu-BCTH ceramics. A weak emission peak centred at 606 nm (around the orange-yellow band) relates to the $^5D_0 \rightarrow {}^7F_1$ electron transition, and a strong emission peak centred at 689 nm (around red band) relates to the $^5D_0 \rightarrow {}^7F_4$ electron transition. Furthermore, the excitation light presents a blue-shift and the emission light of the $^5D_0 \rightarrow {}^7F_1$ transition exhibits a red-shift, which are related to the different ceramics synthesis methods and ferroelectric hosts.

Insets of Fig. 11 show luminescent images of some typical compositions. Owing to limitations of excitation light wavelengths of the Nikon Microscope, the Eu-BCTH ceramics present an orange-yellow color (i.e., weak emission light of 606 nm relating to the $^5D_0 \rightarrow {}^7F_1$ transition). Overall, the luminous spots are homogenously distributed, compensating for the deficiency in the Eu surface distribution detected by EDS. With increasing the Eu content, the luminous intensity of the light spots increases obviously accompanied by an increase in the light points surface density and luminescence spot sizes. It is well known that crystal-field perturbation induced by different host matrices will influence the fluorescent performance of the rare-earth-based phosphors. As compared with the matrices of the NBT powder prepared by the hydrothermal method and the KNN ceramics prepared by the conventional solid-state method [27, 28], the excitation light wavelength, emission peak, and fluorescent lifetime change slightly for the Eu-doped BCTH ceramics; this change can be attributed to the perturbations of crystal-fields of the different matrices.

The strong 689 nm emission peak was used to study the influence of Eu concentration on photoluminescence

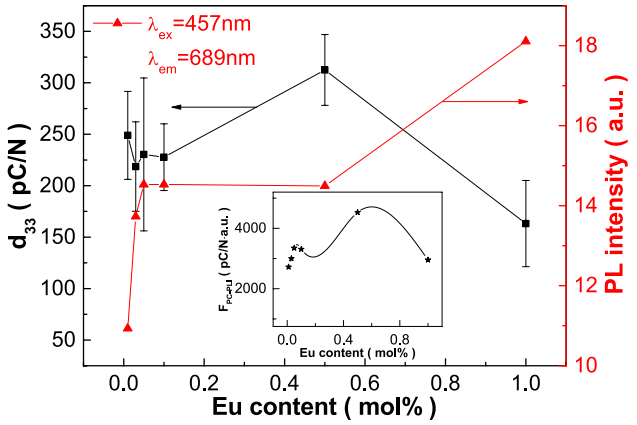

Fig. 12 Variation of piezoelectric constant d_{33} and photoluminescence intensity of the 689 nm emission peak with the Eu content

intensity, as show in Fig. 12. Eu cation doping presents donor doping characteristics in the BCTH system, which tends to increase the d_{33} value and dielectric loss tangent with increasing the Eu content via the point defect reaction $Eu_2O_3 \xrightarrow{BCTH} 2Eu^{\bullet}_{Ba/Ca} + V''_{Ba/Ca} + 3O^{\times}_{O}$. However, when the Eu content is too high, oxygen vacancy is generated via the point defect reaction $2Eu_2O_3 \xrightarrow{BCTH} 4Eu'_{Ti/Ef} + 2V^{\bullet\bullet}_{O} + 4O^{\times}_{O} + O_2 \uparrow$ combined with the evaporation of some cations during the high-temperature sintering, which reunites donor electrons and decreases the piezoelectric constant. Such a change is normal in the donor doped piezoelectric materials; for example, it was reported in the Y_2O_3-doped $Ba_{0.9}Ca_{0.1}Ti_{0.9}Sn_{0.1}O_3$ ceramics [29]. Combined with Fig. 11, it can be seen that the photoluminescence intensity increases sharply between 0.01 mol% and 0.05 mol% with increasing the Eu content. Another rapid increase occurs when the Eu doping content is above 0.5 mol%. The Eu-BCTH ceramics exhibit comparable intensity between 0.05 mol% and 0.5 mol% Eu. However, further increases in the Eu content are insignificant as the piezoelectric constant decreases to unacceptably low values even while the photoluminescence intensity continues to increase. Since piezoelectricity and fluorescence intensity are the most important performances for fluorescent and piezoelectric multifunctional applications, we propose a piezoluminescence figure of merit ($F_{PC-PLI} = d_{33} \times$ PL intensity) referred to Ref. [2] to evaluate the multifunctional performance induced by Eu doping in the BCTH ceramics. The 0.5 mol% Eu-doped BCTH ceramics present excellent piezoelectric and florescent properties (inset of Fig. 12) and offer potential for the development of multifunctional lead-free piezoelectric ceramics.

Figure 13a shows a CIE1931 chromaticity diagram for the Eu-BCTH ceramics. Within the compositional variation of 0.01–1 mol%, the calculated color coordinates

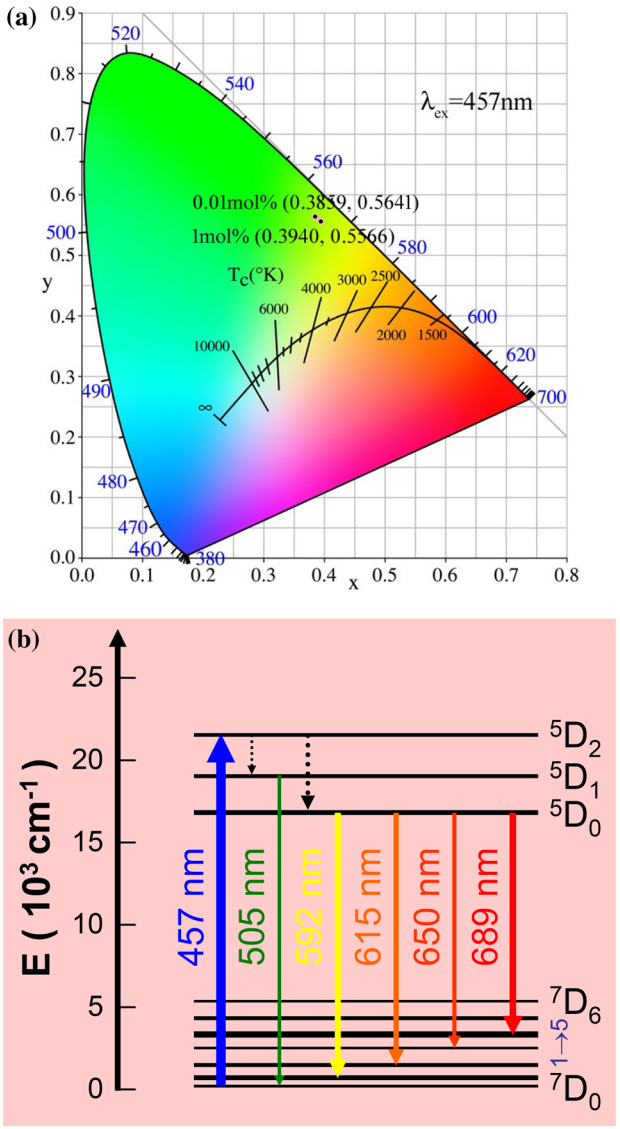

Fig. 13 **a** CIE1931 chromaticity diagram of the Eu-BCTH ceramics with end compositions; **b** schematic diagram of the photoluminescence emitting mechanism induced in the Eu-BCTH ceramics

concentrate at 0.38–0.39 and 0.56–0.55, and overlap under the 457 nm light excitation. The color coordinates locate within the orange-yellow region, which agrees well with the weak photoluminescence emission of the $^5D_0 \rightarrow {}^7F_1$ transition and luminescent images. Figure 13b shows a diagram of the luminescence emitting process of the Eu-BCTH ceramics. Under the 457 nm light excitation, carriers obtain enough energy and are excited from the ground state level $^7F_0$ to the high energy level $^5D_2$ in the Eu^{3+} cations. The excited electrons at the $^5D_2$ level are unstable and relax to the low energy levels $^5D_1$ and $^5D_0$ via non radiative process. The weak orange-yellow fluorescence at 606 nm and strong red fluorescence at 689 nm (Fig. 11) can be

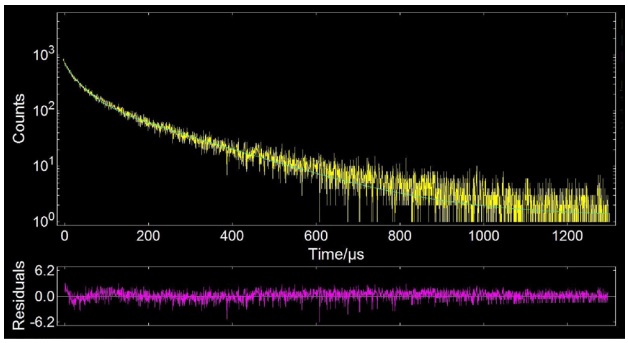

Eu content (mol%)	τ_1 (μs)	τ_2 (μs)	χ_2
0.01	31.18	157.26	1.140
0.5	33.94	178.64	1.239
1	54.11	265.48	1.139

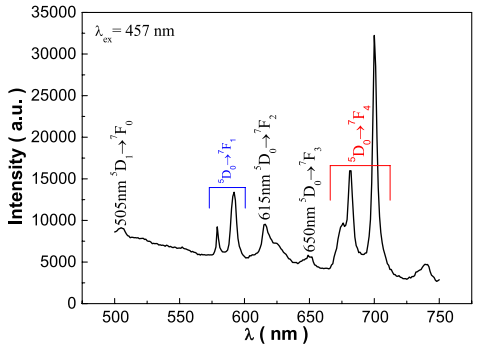

Fig. 14 Decay curve of the 0.5 mol % Eu-doped BCTH ceramics. Insets show the fitting parameters of lifetime of three typical compositions and high-resolution photoluminescence emission spectrum of the 0.5 mol % Eu-doped BCTH ceramics

attributed to the jump from the $^5D_0$ level to the $^7F_1$ electron transition and $^7F_4$ electron transition, respectively [7, 30].

Figure 14 shows the fluorescence decay curve of the 0.5 mol% Eu-doped BCTH ceramics. The photoluminescence lifetime of the Eu^{3+}: $^5D_0 \rightarrow {}^7F_4$ transition can be determined by fitting the exponential characteristic decay curve. Although luminescence lifetime with several tens of microseconds magnitude is obtained for all Eu-doped BCTH ceramics, apparent increases occur with increasing the Eu content. An additional fluorescence decay with 1–2 hundreds of microseconds lifetime and with a similar increasing trend is also observed; this has not been detected before [30, 31]. The second fluorescence lifetime may be correlated with the fine $^5D_0 \rightarrow {}^7F_4$ transitions detected in the high-resolution emission spectra, as shown in the inset of Fig. 14, which contain two apparent emission peaks and one vague peak shoulder. Additional photoluminescence emission peaks are also detected, and correlate with the electron transitions of $^5D_1 \rightarrow {}^7F_0$, $^5D_0 \rightarrow {}^7F_2$, and $^5D_0 \rightarrow {}^7F_3$; the emission mechanism is also shown in Fig. 13b.

4 Conclusions

Near-pure perovskite Eu-BCTH lead-free multifunctional ceramics were prepared by the conventional ceramic processing. The compositions were located around MPB, where doublet splitting of the {200} diffraction reflection and triplet splitting of the {310} diffraction reflection appear with varying Eu doping contents. The Eu-doped BCTH ceramics present complicated dielectric behaviour, and the dielectric response can be fitted by both Curie–Weiss law and exponential law, but all presenting apparent deviation. Excellent electrical and fluorescent properties are obtained for the 0.5 mol% Eu-doped BCTH ceramics, which exhibit relatively large ε_m values, high T_C, perfect ferroelectricity, large d_{33} value, and large fluorescence intensity. Therefore, multifunctional lead-free BCTH ceramics can be developed via rare earth doping, in which piezoelectric and fluorescent properties can be tailored simultaneously.

Acknowledgements This work was supported by the National Natural Science Foundation of China (No. 51577015), the Applied Basic Research Programs of Changzhou (No. CJ20179020), the Top-notch Academic Programs Project of Jiangsu Higher Education Institutions, and the Priority Academic Program Development of Jiangsu Higher Education Institutions. Shanshan Zhang thanks the Postgraduate Research & Practice Innovation Program of Jiangsu Province (No. KYCX19_1753) for financial support.

References

1. K.R. Kandula, K.R. Kandula, S. Asthana, S.S.K. Raavi, Multifunctional Nd^{3+} substituted $Na_{0.5}Bi_{0.5}TiO_3$ as lead-free ceramics with enhanced luminescence, ferroelectric and energy harvesting properties. RSC Adv **8**(28), 15282–15289 (2018)
2. A.D.B.L. Ferreira, P.R.O. Nóvoa, A.T. Marques, Multifunctional material systems: a state-of-the-art review. Compos. Struct. **151**, 3–35 (2016)
3. X. Tian, Z. Wu, Z. Wu, Y. Jia, J. Chen, R.K. Zheng, Y. Zhang, Y. Zhang, H. Luo, Remanent-polarization-induced enhancement of photoluminescence in Pr^{3+}-doped lead-free ferroelectric $(Bi_{0.5}Na_{0.5})TiO_3$ ceramic. Appl. Phys. Lett. **102**(4), 042907 (2013)
4. D.K. Khatua, A. Kalaskar, R. Ranjan, Tuning photoluminescence response by electric field in electrically soft ferroelectrics. Phys. Rev. Lett. **116**(11), 117601 (2016)
5. F. Auzel, Upconversion and anti-stokes processes with f and d Ions in solids. Chem. Rev. **104**(1), 139–173 (2004)
6. H. Dong, L. Sun, C. Yan, Energy transfer in lanthanide upconversion studies for extended optical applications. Chem. Soc. Rev. **44**(6), 1608–1633 (2015)
7. K. Binnemans, Interpretation of europium (III) spectra. Coordin. Chem. Rev. **295**(1), 1–45 (2015)
8. P. Du, L. Luo, J.S. Yu, Energy back transfer induced color controllable upconversion emissions in La_2MoO_6:Er^{3+}/Yb^{3+} nanocrystals for versatile applications. Part. Part. Syst. Charact. **35**(3), 1700416 (2018)
9. W. Kleemann, Random fields in relaxor ferroelectrics—a jubilee review. J. Adv. Dielect. **2**(2), 1241001 (2012)

10. C. Zhou, W. Liu, D. Xue, X. Ren, H. Bao, J. Gao, L. Zhang, Tripe-point-type morphotropic phase boundary based large piezoelectric Pb-free material $Ba(Ti_{0.8}Hf_{0.2})O_3$–$(Ba_{0.7}Ca_{0.3})TiO_3$. Appl. Phys. Lett. **100**(22), 222910 (2012)
11. D. Wang, Z. Jiang, B. Yang, S. Zhang, M. Zhang, F. Guo, W. Cao, Phase transition behavior and high piezoelectric properties in lead-free $BaTiO_3$-$CaTiO_3$-$BaHfO_3$ ceramics. J. Mater. Sci. **49**(1), 62–69 (2014)
12. C. Zhao, W. Wu, H. Wang, J. Wu, Site engineering and polarization characteristics in $(Ba_{1-y}Ca_y)(Ti_{1-x}Hf_x)O_3$ lead-free ceramics. J. Appl. Phys. **119**(2), 024108 (2016)
13. Z. Wang, W. Li, R. Chu, J. Hao, G. Li, Structure and piezoelectric properties of $(Ba_{1-x}Ca_x)(Ti_{0.95}Hf_{0.05})O_3$ lead-free ceramics. Mater. Res. Bull. **97**, 334–342 (2018)
14. J. Sun, B. Fang, S. Zhang, Z. Chen, J. Ding, X. Zhao, H. Luo, Upconversion and downconversion luminescence properties of Er^{3+} doped NBT ceramics synthesized via hydrothermal method. Opt. Mater. **69**, 244–249 (2017)
15. J. Shi, J. Sun, B. Fang, Q. Du, S. Zhang, J. Ding, Photoluminescence performance of Er/Yb co-doped NBT ceramics prepared via hydrothermal method. J. Phys. Chem. Solids **121**, 228–235 (2018)
16. X. Liu, D. Wu, Z. Chen, B. Fang, J. Ding, X. Zhao, H. Luo, Ferroelectric, dielectric and pyroelectric properties of Sr and Sn co-doped BCZT lead free ceramics. Adv. Appl. Ceram. **114**(8), 436–441 (2015)
17. D.S. Keeble, F. Benabdallah, P.A. Thomas, M. Maglione, J. Kreisel, Revised structural phase diagram of $(Ba_{0.7}Ca_{0.3}TiO_3)$–$(BaZr_{0.2}Ti_{0.8}O_3)$. Appl. Phys. Lett. **102**(9), 092903 (2013)
18. S.-Y. Liu, Y. Meng, S. Liu, D.-J. Li, Y. Li, Y. Liu, Y. Shen, S. Wang, Compositional phase diagram and microscopic mechanism of $Ba_{1-x}Ca_xZr_yTi_{1-y}O_3$ relaxor ferroelectrics. Phys. Chem. Chem. Phys. **19**(33), 22190–22196 (2017)
19. M.B. Abdessalem, S. Aydi, A. Aydi, N. Abdelmoula, Z. Sassi, H. Khemakhem, Polymorphic phase transition and morphotropic phase boundary in $Ba_{1-x}Ca_xTi_{1-y}Zr_yO_3$ ceramics. Appl. Phys. A **123**(9), 583 (2017)
20. R.D. Shannon, Revised effective ionic radii and systematic studies of interatomic distances in Halides and chalcogenides. Acta Crystallogr. A **32**, 751–767 (1976)
21. L. Luo, P. Du, P. Du, W. Li, H. Chen, H. Chen, Effects of Er doping site and concentration on piezoelectric, ferroelectric, and optical properties of ferroelectric $Na_{0.5}Bi_{0.5}TiO_3$. J. Appl. Phys. **114**(12), 124104 (2013)
22. X. Liu, B. Fang, J. Deng, H. Deng, H. Yan, Q. Yue, J. Chen, X. Li, J. Ding, X. Zhao, H. Luo, Phase transition behavior and defect chemistry of [001]-oriented $0.15Pb(In_{1/2}Nb_{1/2})O_3$–$0.57Pb(Mg_{1/3}Nb_{2/3})O_3$–$0.28PbTiO_3$–Mn single crystals. J. Appl. Phys. **117**(24), 244102 (2015)
23. W. Ji, S. Feng, B. Fang, X. Zhao, S. Zhang, J. Ding, H. Luo, Facile preparation and performance of novel high-T_C $xBi(Ni_{1/2}Ti_{1/2})O_3$–$(1-x)Pb(Zr_{1/2}Ti_{1/2})O_3$ piezoceramics. Curr. Appl. Phys. **18**(3), 289–296 (2018)
24. B. Fang, M. Zhu, J. Ding, Y. Shan, H. Imoto, Improving ferroelectric and piezoelectric properties of $PbFe_{1/4}Sc_{1/4}Nb_{1/2}O_3$ ceramics by oxide doping prepared via a B-site oxide mixing route. Ceram. Int. **39**(2), 1677–1681 (2013)
25. R. Zhu, Y. Yin, B. Fang, Z. Chen, S. Zhang, J. Ding, X. Zhao, H. Luo, Optimizing structure and electrical properties of high-Curie temperature PMN-PHT piezoelectric ceramics via tailoring sintering process. Eur. Phys. J. Appl. Phys. **74**(3), 30101 (2016)
26. H. Liu, J. Chen, H. Huang, L. Fan, Y. Ren, Z. Pan, J. Deng, L.Q. Chen, X. Xing, Role of reversible phase transformation for strong piezoelectric performance at the morphotropic phase boundary. Phys. Rev. Lett. **120**(5), 055501 (2018)
27. J. Sun, P. Chen, B. Fang, S. Zhang, J. Ding, Hydrothermal synthesis and luminescence properties of NBT-Eu nanopowders. Chin. J. Lumin. **37**, 151–157 (2016). **(in Chinese)**
28. J.A. Peña-Jiménez, F. González, R. López-Juárez, J.M. Hernández-Alcántara, E. Camarillo, H. Murrieta-Sánchez, L. Pardo, M.E. Villafuerte-Castrejón, Optical and piezoelectric study of KNN solid solutions co-doped with La–Mn and Eu–Fe. Materials **9**(10), 805 (2016)
29. Z.H. Chen, Z.W. Li, J.H. Qiu, T.X. Zhao, J.N. Ding, X.G. Jia, W.Q. Zhu, J.J. Xu, J.J. Xu, Y_2O_3 doped $Ba_{0.9}Ca_{0.1}Ti_{0.9}Sn_{0.1}O_3$ ceramics with improved piezoelectric properties. J. Eur. Ceram. Soc. **38**(4), 1349–1355 (2018)
30. J. Hao, Z. Xu, R. Chu, W. Li, P. Fu, J. Du, G. Li, Large electrostrictive effect and strong photoluminescence in rare-earth modified lead-free $(Bi_{0.5}Na_{0.5})TiO_3$-based piezoelectric ceramics. Scripta Mater. **122**, 10–13 (2016)
31. H. Sun, Q. Zhang, X. Wang, M. Gu, A new red-emitting material $K_{0.5}Na_{0.5}NbO_3$:Eu^{3+} for white LEDs. Mater. Res. Bull. **64**, 134–138 (2015)